Journal of MATERIALS RESEARCH

Invited Paper
DOI:10.1557/s43578-022-00550-0

ADVANCES IN TITANIUM BIO-IMPLANTS

FOCUS ISSUE

Sol–gel derived hydroxyapatite coating on titanium implants: Optimization of sol–gel process and engineering the interface

Alaa Jaafar[1,2], Christian Schimpf[3], Marcel Mandel[4], Christine Hecker[1,2], David Rafaja[3], Lutz Krüger[4], Pal Arki[1,2,a], Yvonne Joseph[1,2]

[1] Institute of Electronic and Sensor Materials, TU Bergakademie Freiberg, Freiberg, Germany
[2] Center for Efficient High Temperature Processes and Materials Conversion, TU Bergakademie Freiberg, Freiberg, Germany
[3] Institute of Materials Science, TU Bergakademie Freiberg, Freiberg, Germany
[4] Institute of Materials Engineering, TU Bergakademie Freiberg, Freiberg, Germany
[a] Address all correspondence to this author. e-mail: Pal.Arki@esm.tu-freiberg.de

Received: 15 February 2022; accepted: 1 April 2022; published online: 27 April 2022

Sol–gel derived hydroxyapatite coatings on metallic implants are important to promote their osseointegration and biocompatibility. However, such coatings generally suffer from drawbacks that limit implant longevity. In this study, the sol gel process to prepare hydroxyapatite was optimized and used to deposit a hydroxyapatite layer on Ti6Al4V. Samples were pretreated by thermal oxidation, sol–gel coating, and anodization to produce titanium dioxide interlayers with various structures. The results of structural and thermal analysis have determined the optimal preparation parameters to produce monophasic and crystalline hydroxyapatite. The introduction of titanium dioxide intermediate layers produced crack-free hydroxyapatite films and promoted the adherence and integrity of the coating, where the adhesive strength was remarkably improved. Furthermore, potentiodynamic polarization tests in simulated body fluid revealed low corrosion rates and high protection property of the hydroxyapatite/titania coated samples, making these structures promising for the coatings of bone replacements.

Introduction

Titanium (Ti) and its alloys are widely used as implants to substitute damaged load-bearing bones due to their unique combination of excellent corrosion resistance, high mechanical strength, low density and high biocompatibility [1–3]. However, there are still limitations associated with implanting these types of biomaterials including their bio-inertness that can inhibit bone tissues growth, release of undesirable ions, severe adhesive wear to bone and induction of stress shielding [4–7]. In this regard, surface modification by deposition of hydroxyapatite (HA) could provide many biological benefits and minimize the limitations of Ti implants [8]. Deposition of HA could be implemented by several techniques including sol–gel method, plasma spraying, electrophoretic deposition and pulsed-laser deposition. Among these techniques, sol-gels have gained much attention over the last years due to its advantages over other coating techniques, e.g. low processing temperature, low cost, and the ability to produce pure and homogenous HA coatings [9].

Synthesis of pure HA via sol–gel method involves several stages: (1) preparation of the sol using suitable precursors, e.g. metal alkoxides or metal salts, (2) gelation where adequate polymerization takes place to form cross-linking of molecules, (3) aging that is important for purity [10, 11] and (4) drying to remove excess solvent. Finally, a heat treatment is performed to eliminate organic compounds and to achieve crystallization. To produce HA coatings, the aged sol is deposited on the substrate by either spray, spin or dip coating and treated afterwards with different drying and sintering procedures. Inaccurate preparation conditions could produce non-biocompatible contaminant phases [12], poorly crystallized HA which is unstable and could be decomposed in the body [13] or formation other calcium phosphate phases [14]. In literature, several studies have been developed to form pure HA [14–19]. However, with such a wide variety of processing conditions, selection of a specific route for HA preparation with defined characteristics is difficult. Hence, determining the optimum experimental variables for

the adopted preparation formula of HA sol is important before coating.

In spite of the biological enhancements that HA coatings could provide to Ti alloys surfaces, there are still many concerns about their use. The difference in the thermal expansion coefficient (CTE) between Ti6Al4V (8.9×10^{-6} K^{-1}) and HA (15×10^{-6} K^{-1}) limits the adhesive strength between them and promotes surface defects after sintering, which causes detachment and delamination under loading in the physiological environment. In addition, insufficient corrosion resistance of pure HA coatings, as reported previously [1], raises concerns for long-term reliability. To overcome these challenges, introduction of interlayers, titanium dioxide (TiO_2) in particular, has been reported as an efficient way to improve the adhesion of HA layers and improve corrosion behavior.

Many studies have been carried out to form a TiO_2 sol–gel interlayer and investigate their impact on the HA coatings. Kim et al. [20] observed an improvement in adhesion of HA layer by 60% after introduction of a TiO_2 interlayer. Balakrishnan et al. [21], found that adhesive strength could be increased from 15.8 ± 7 MPa to 40.3 ± 3 MPa after introduction of TiO_2. In addition, Azari et al. [22] and Xu et al. [23] observed in their investigations that introduction of sol–gel TiO_2 interlayers could improve the coating cohesion and eliminate delamination at the interface compared to single HA coatings. From the electrochemical perspective, Hussein and Mohammed [24] reported an enhancement in corrosion performance for the TiO_2-HA bilayer by 63% and 32% compared to uncoated and TiO_2 coated specimens, respectively.

Other scientists suggested anodization rather than sol–gel coating as the anodization process is an effective way to create various morphologies of TiO_2 on Ti surfaces with precise control of the film thickness. Roest et al. [25] have successfully created rough TiO_2 layers via anodization and observed improvement in bonding strength on the HA coating. This improvement is not only limiting the difference of thermal expansion coefficient between Ti and HA, but the roughness of the TiO_2 could increase the wettability of the HA sol and subsequently improve the adhesive strength of HA layer based on mechanical interlocking. In similar studies, nanotube structures of TiO_2 interlayers have been prepared by anodization using fluoride-containing electrolyte. Ji et al. [26], Robertson et al. [27] and Kang et al. [28] reported in their investigations that introducing this type of layer could remarkably improve the adhesion, electrochemical properties and contribute to producing a crack-free HA coating. Thermal oxidation has been also considered to form TiO_2 as an interlayer. Production of these types of layers, and their benefits on the HA coatings, have been well reviewed previously by Baddar et al. [29]. While the previously mentioned studied have experimented with different methods of TiO_2 interlayer formation, the effect on hydroxyapatite coatings has not been compared systematically and the optimal method has not yet been identified.

In the present study, TiO_2 intermediate layers prepared by various methods such as sol–gel, anodization, and thermal oxidation, were compared. The microstructure, thickness, surface roughness and morphology of these layers were investigated. Furthermore, critical parameters of the HA sol preparation, including pH value of sol, aging time and sintering temperature have been investigated. The optimal HA sol was deposited on pure and TiO_2 treated Ti6Al4V alloy substrates. The microstructure of these samples were evaluated and the bonding strength, wettability to simulated body fluid (SBF) and corrosion resistance have been investigated.

Results and discussion

Hydroxyapatite powders prepared by sol–gel process

An ethanol-based sol–gel process was used to prepare hydroxyapatite powders. The X-ray diffraction patterns of the HA powder prepared with different aging times and pH levels and their phase compositions are shown in Fig. 1. As can be observed, aging the sol for 24 h at pH of 5.9 based on the formula adopted in this study was sufficient to produce crystalline HA (JCPDS card No. 9–0432, SG P63/m) and there was no sign of other crystalline calcium phosphate phases. The hydrolyzed Ca sol (possibly in form of $Ca(OEt)_x(NO_3)_{2-x}$) interacted with the P sol (generally in form of $P(OEt)_{3-y}(OH)_y$) to form Ca-O-P bonds during aging as demonstrated in the following reaction [30, 31]:

$$P(OEt)_{3-y}(OH)_y + Ca(OEt)_x(NO_3)_{2-x} \rightarrow (OEt)_{x'}(NO_3)_{2-x'} - Ca - O - HPO(OEt)_{3-y'} + H_2O + C_2H_5OH \quad (1)$$

However, presence of calcium oxide (CaO, SG $Fm\bar{3}m$) diffraction lines at 37.38 and 53.9° were also detected, especially for samples with shorter aging times. Here, a lack of Ca-O-P linkage formation occurs due to incomplete reaction, which results in formation of the CaO phase [32]. The presence of this phase is undesirable, since it is not biocompatible and could degrade shortly after implantation due to its high solubility in body fluid [23]. In addition, the decomposition of this compound increases the susceptibility of cracks formation by dissolving and releasing of gases that could produce non-stoichiometric HA layer. Furthermore, CaO is a strong base compound with serious cytotoxic effect, which could cause severe inflammation upon its dissolving in the body fluid [33]. Therefore, a reduction the quantity of CaO in the HA structure is important to maintain its biocompatibility. As demonstrated in Fig. 1, increasing the

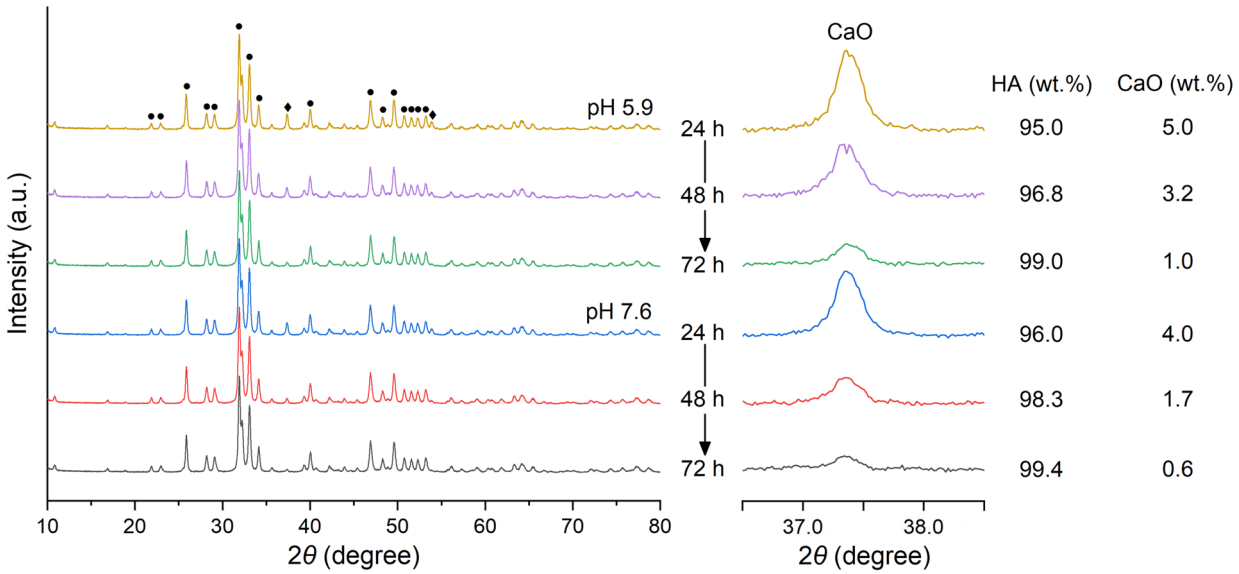

Figure 1: XRD pattern of sol–gel HA powder. The legends are: (filled circle) HA and (filled diamond) CaO.

aging time at pH 5.9 eliminates the presence of the CaO phase within the detection limit of XRD (here around 1%). However, increasing the aging time in solutions with pH 7.6 was more efficient at reducing the presence of the CaO phase, until reaching 99.4% purity of HA at 72 h of aging time. This suggests that these parameters are optimal to produce nearly monophasic HA. Increasing the aging time up to 72 h is important to complete the polymerization and condensation reactions in the gel and removing any undesirable phases, while increasing the pH of solution up to 7.6 could accelerate the achievement of pure HA as described previously [16]. It is worth mentioning that aging more than 72 h is not recommended as the HA could be decomposed to tricalcium phosphate (TCP) and CaO due to the extra removal of structural water [34]. The XRD pattern of TiO_2 prepared by sol–gel, shown in Fig. S-1 (supporting information), indicated a high compositional purity of TiO_2 with a mixture of rutile (JCPDS # 21-1276) and anatase (JCPDS # 21-1272) crystalline structure.

The FTIR spectra of the HA powder synthesized under different conditions are presented in Fig. 2. The bands at 962, 1044 and 1091 cm^{-1} were assigned to the stretching mode of phosphate group, whereas the bands at 569 and 602 cm^{-1} were assigned to the bending vibration mode of O–P–O linkage in the phosphate group [35]. The peaks at 630 and 3567 cm^{-1} were attributed to the vibrational modes of the hydroxyl group, which indicated the crystalline nature of HA [36]. The broad band in the range of 3300–3600 cm^{-1} and the peak at 1638 cm^{-1} are related to O–H group stretch vibration of absorbed water. The band at 1384 cm^{-1} and low intensity peak at 875 cm^{-1} represent asymmetric stretching of the C–O

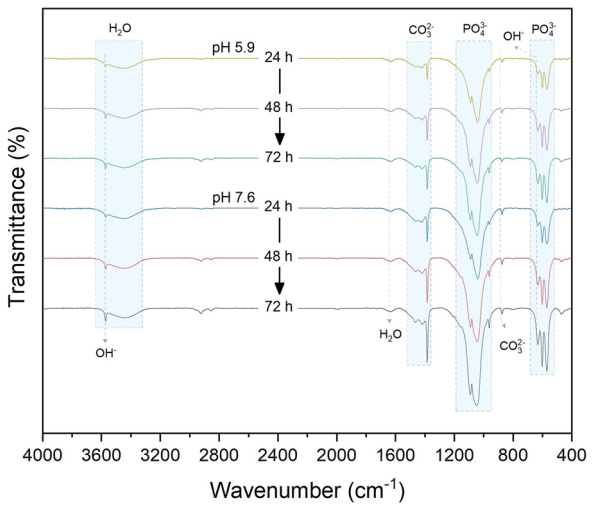

Figure 2: FTIR spectra of sol–gel HA powder prepared under various conditions.

bond of the carbonate group (CO_3^{2-}) indicating that carbonate substitution had occurred at a certain level. Carbonate incorporation is a common phenomenon during biological apatite formation and considered preferential in the human bone due to its excellent bioactivity and osteoinductivity [37]. However, the peak at 876 cm^{-1} could also indicate the presence of acidic phosphate groups (HPO_4^{2-}) in the system due to the stretching vibration of P-OH linkage [38, 39]. Nevertheless, no other HPO_4^{2-} species were detected in the spectra. No significant changes in the shapes and intensities of the peaks were observed for any of the samples, which indicates that varying the studied synthesis condition does not change the

asymmetric vibration modes of the main functional groups (PO_4^{-3}, OH^-). This conclusion is in agreement with the observations of XRD analysis.

The thermal behavior of the HA dried gel prepared under optimal conditions (72 h, pH 7.6) based on DSC/TG analysis is shown in Fig. 3. Two stages of low and high sintering temperatures are detected. The endothermic peak at 60 ℃ points to the evaporation of absorbed water. The exothermic peaks at 99 and 185 ℃ associated with losing 13% weight are attributed to the decomposition of organics and nitrates. The last endothermic peak at 580 ℃ with associated 40% weight loss of indicates the HA phase crystallization. After 580 ℃, slight and constant weight loss and no thermal behavior were indicated. A total weight loss of 44% due to the evaporation of absorbed water, decomposition and burning of organics and nitrates and crystallization is observed in the process. Hence, the DSC/TG analysis indicates that 600 ℃ is an optimum sintering temperature to decompose organics and nitrates substances and produce crystalline HA.

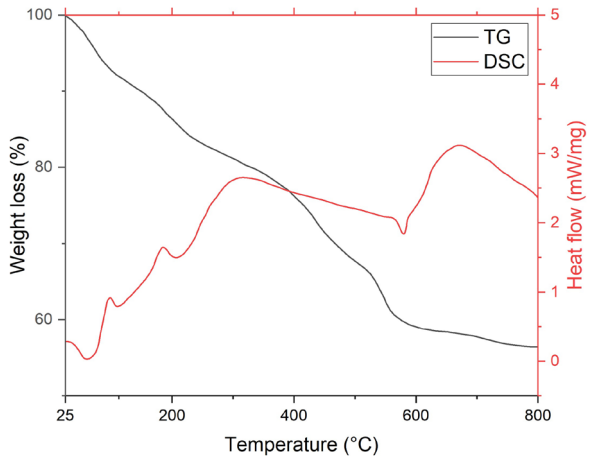

Figure 3: DSC/TG curves of HA dried gel heated under atmospheric conditions.

Based on the XRD, FTIR and DSC/TG results, the aging time of 72 h, 7.9 pH value and sintering temperature of 600 ℃ have been determined as the optimum parameters to prepare HA coatings according to the used sol.

TiO_2 Layers on Ti6Al4V

Figure 4 shows the SEM micrographs of the surface of the Ti6Al4V alloy and the TiO_2 layers formed on it via various methods. The thickness, surface roughness and wettability of the TiO_2 treated and the untreated samples are indicated in Table 1.

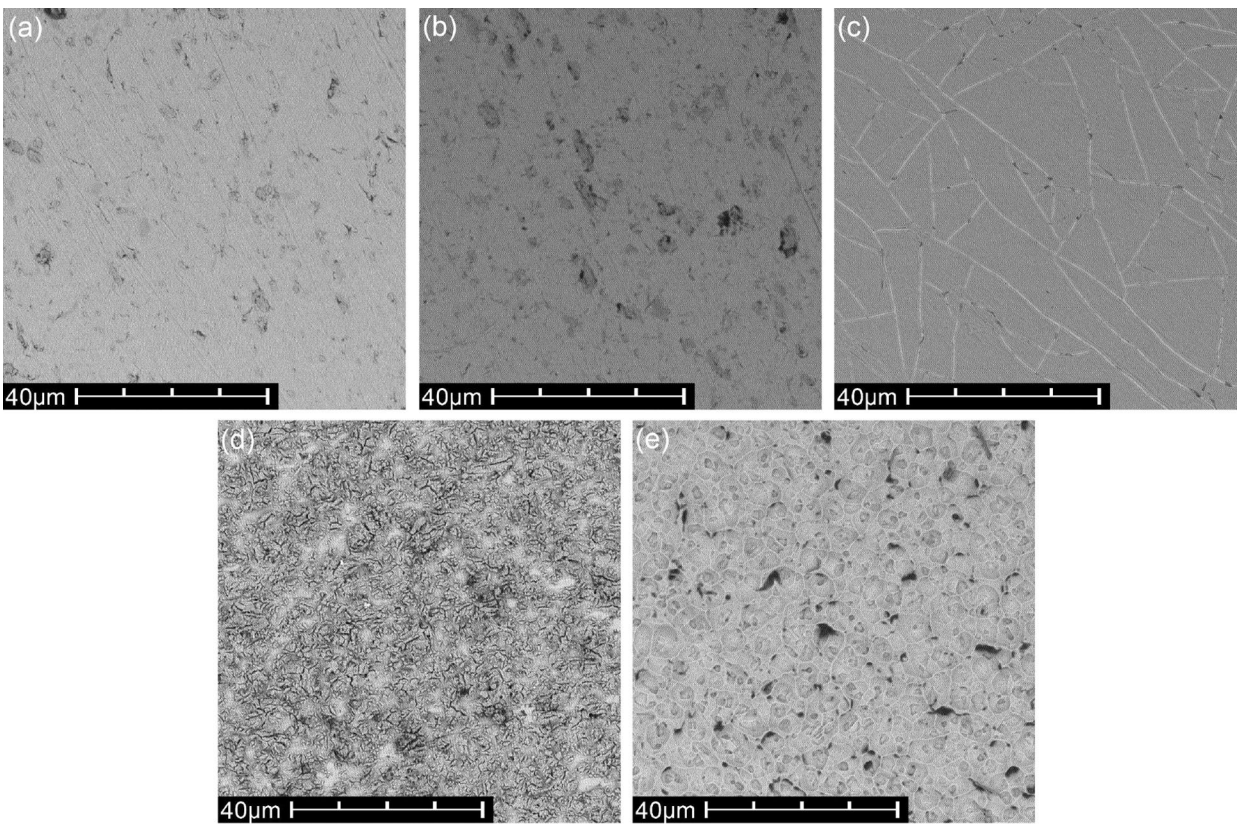

Figure 4: SEM micrographs of the surface structures of: (a) Ti6Al4V, (b) T1, (c) T2, and (d) T3, (e)T4.

TABLE 1: Thickness, surface roughness and contact angle of bare and TiO_2 treated Ti alloy.

Properties	Ti6Al4V	T1	T2	T3	T4
Thickness (nm)		138 ± 14	216 ± 19	108 ± 8	174 ± 13
Surface roughness (nm)	51 ± 13	84 ± 19	126 ± 23	187 ± 47	152 ± 32
Contact angle (°)	73 ± 1	68 ± 2	63 ± 3	57 ± 2	59 ± 3

The thermal oxidation process produced a uniform TiO_2 layer [Fig. 4(b)], no cracks appeared in the structure of this layer. A slight improvement in surface roughness (64.7%) and wettability (11.7%) was observed after introduction of this layer. On other hand, the presence and distribution of cracks for the TiO_2 formed by sol–gel coating could be observed from Fig. 4(c). These cracks are formed due to the mechanical constraints occurring during the heat treatment process due to the difference in the thermal expansion coefficients of TiO_2 (11.8×10^{-6} K^{-1}) and Ti6Al4V surface. However, these cracks could be beneficial, as the HA coating could penetrate these cracks and subsequently improve the adhesion strength of the HA layer based on mechanical interlocking theory as reported previously by Wen et al. [40]. This layer has the highest thickness compared to other produced layers, while its surface roughness and wettability increased by 147% and 18.2%, respectively, compared to polished Ti alloy. Anodization with H_2SO_4 electrolyte produced a micro porous and highly rough structure of TiO_2 layer, while the anodization of Ti alloy with fluoride-containing electrolyte produced a rough and nanotube structure of TiO_2 layer. The micro-pores are possibly created due to exceeding the dielectric potential limit of the oxide and generating sparks with very high temperatures resulting in local melting processes. The presence of micro-pores, nano-pores, and the rough TiO_2 structure could improve the quality of the HA coating by HA penetration, providing better adhesion and bonding strength according to mechanical interlocking. The T3 samples showed the highest surface roughness and wettability compared to the other TiO_2 layers, which promises good wetting and bonding.

Hydroxyapatite layers on Ti6Al4V and TiO_2/Ti6Al4V

SEM images of the HA layers directly deposited on Ti6Al4V substrate after heat treatment is shown in Fig. 5(a). Micro-cracks were distributed in the HA layer, which is again mainly due to the mismatch in the thermal expansion coefficients. The difference in the thermal expansion coefficient of Ti6Al4V and HA induces residual tensile stress on the HA layer during the sintering process leading to crack formation. Figure 5(b) and (c) show the surface morphology of the HA coating after soaking in SBF for 21 days at various magnifications. The morphology of the coating surface shows a precipitation of white particles, which indicate formation of apatite on the pure HA layers. XRD analysis was performed to this sample and only HA and Ti phases were observed proving that precipitated layer is apatite and confirming the good bioactivity of the HA coating in SBF.

The SEM images of sol–gel HA structure coated on TiO_2 interlayers are shown in Fig. 6. The thicknesses of the HA layers are ranging from 3 to 5 μm and are entirely covering the surfaces as no TiO_2 was detected. Contrary to the many cracks that appeared in the HA coating of untreated Ti6Al4V [compare Fig. 5(a)], the introduction of the TiO_2 interlayer by thermal oxidation showed only a limited number of cracks on the HA film [Fig. 6(a)], and no cracks were apparent in any of the other samples. Hence, the role of the TiO_2 interlayer in reducing the thermal expansion coefficient difference between the Ti alloy and HA layer, as well as enhancement of mechanical interlocking of the film and substrate, is demonstrated. Furthermore, the outer surface of the HA layer shows a rough structure, especially

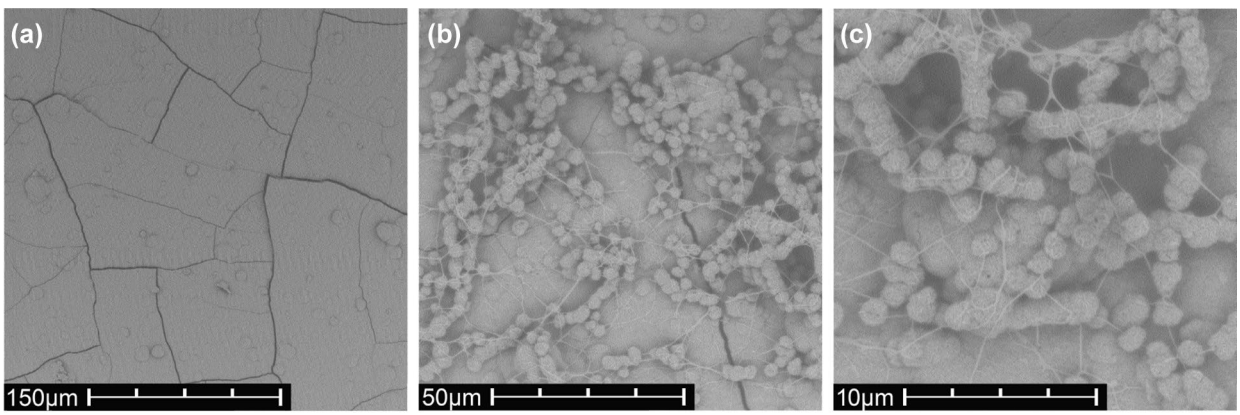

Figure 5: SEM micrographs of: (a) HA film surface structures and (b), (c) after soaking in SBF for 21 days.

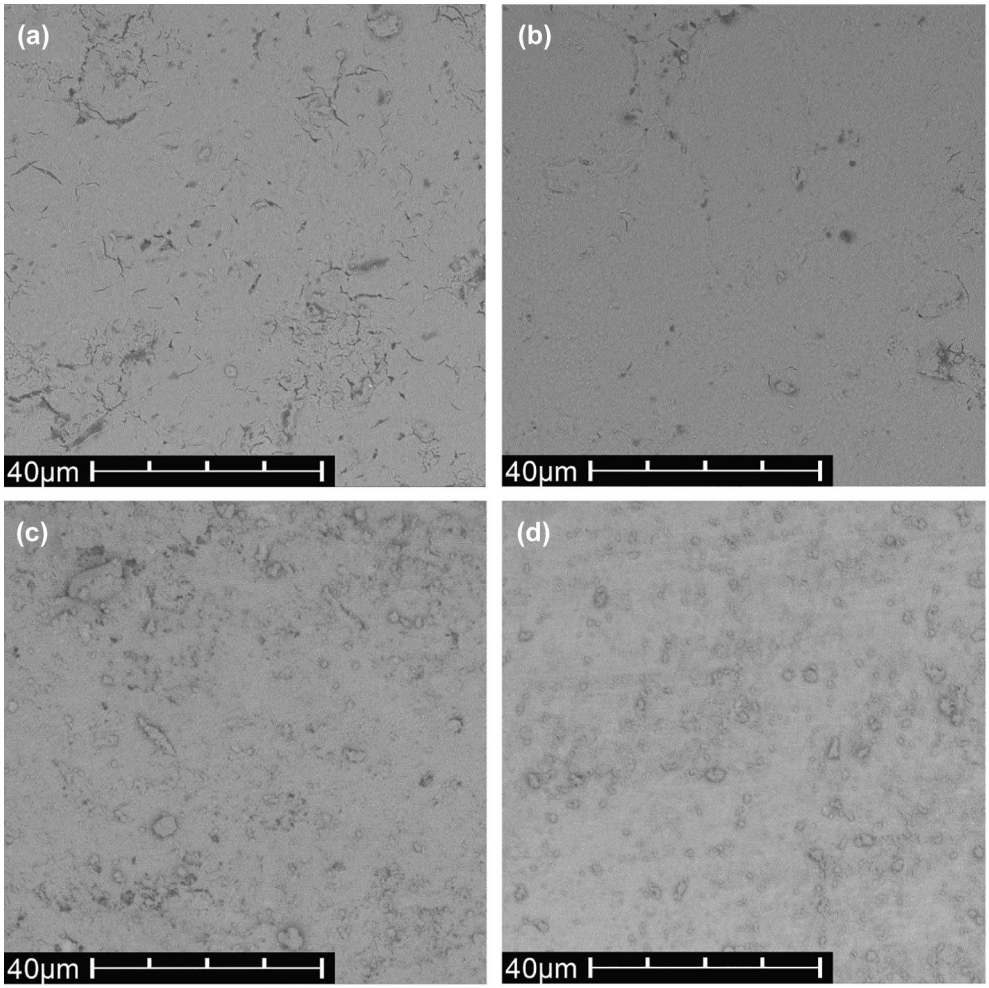

Figure 6: SEM observations of HA coatings in samples (a) HAT1, (b) HAT2, (c) HAT3, (d) HAT4.

for HAT3 and HAT4. This roughness could be formed during the sintering temperature due to the decomposition of organic materials. The rough structure has higher specific surface area for interlocking of the coating material, which is expected to provide more susceptible to the natural remodeling processes and accelerates the fixation of the coated implant with surrounding bones.

The wettability test based on contact angle measurements with SBF was conducted on the applied coatings to evaluate their ability to interact favorably with the biological environment as presented in Table 2 and Fig. S-2 (supporting information). Hence, when compared to the wettability of coated samples, the uncoated surface of the Ti alloy exhibits a higher hydrophobic nature, as it shows the highest contact angle of 73° ± 1°. On the other hand, all HA coated samples showed hydrophilic nature. Introduction of the TiO_2 interlayers slightly improved the hydrophilicity of the HA coating, as a decrease in contact angle was noticed. It has been suggested that hydrophilic surfaces have better cell adhesion compared to the surfaces with hydrophobic nature [41]. In addition, the hydrophilic nature of coatings improves the hydroxyapatite formation and growth due to the enhancement of ion exchange behavior from body fluid

TABLE 2: Contact angle and adhesive strength of HA coatings on TiO_2 treated and bare Ti alloy.

Properties	Ti6Al4V	HA	HAT1	HAT2	HAT3	HAT4
Adhesive strength (MPa)		14.31 ± 1.6	17.11 ± 2.2	$23.40 \pm 2.5^{*,\#\#}$	$25.23 \pm 2.7^{*,\#\#}$	$21.73 \pm 2.4^{*,\#}$
Contact angle (°)	$73 \pm 1^{*,\#\#}$	56 ± 2	49 ± 2*	$45 \pm 3^{*,\#\#}$	$41 \pm 2^{*,\#\#}$	$43 \pm 2^{*,\#\#}$

Statistically significant differences were indicated as $^{*}p < 0.01$ compared with HA coating and $^{\#}p < 0.05$, $^{\#\#}p < 0.01$ compared with HAT1 coating.

[42]. Accordingly, surface pre-treatment by formation of TiO_2 interlayer are increasing the SBF interaction area with the outer HA coating leading to the acceleration of the osseointegration, i.e., the structural connection between the HA coated implant and living bone.

High adhesion strength of HA coatings is an important property affecting the durability and longevity of the Ti implants, especially in load-bearing conditions. Hence, the introduction of TiO_2 as intermediary layer represents an excellent practical solution to achieve higher adhesion by improving the morphological properties of the outer layer and to reduce the strain in the coating/substrate interface that could occur during the calcination process. The adhesive bond strengths of the HA layers to the Ti alloy surfaces are given in Table 2 as function of the intermediate layer type and shown in Fig. S-3 (supporting information). The minimum bonding strength is noted in the HA coating (14.3 ± 1.6 MPa) on the untreated Ti6Al4V. The failure mode is observed to be mostly an adhesive fracture due to the cracks presented in this coating that could cause a delamination at the interface. Similar values of adhesion strength for the pure HA coating were reported previously [21, 27].

Formation of TiO_2 interlayer improved the adhesion. The thermal oxidation of Ti substrate has slightly improved the adhesion of HA coating. The adhesive fracture mode is still dominant, but a minor part of this coating has shown a cohesive failure. However, this improvement is statistically insignificant. Meanwhile, the anodized and sol–gel TiO_2 interlayers have shown significant improvement of adhesion strength of about 63.6% for HAT2, 76.2% for HAT3 and 51.7% for HAT4 compared to the coating on the untreated Ti6Al4V. The failure type of the coating in these samples was a mixed mode of adhesive and cohesive fracture, where delamination of coating (referring to the adhesive failure mode) and islands of residual coating materials on both sides of post and substrate surface were detected. The change of failure mode in the bilayer coatings could be associated with alteration of adhesive failure location, whereas the single HA layers fail through HA/substrate interface, while the bilayer coatings could fail only through the interface of HA layer and TiO_2 interlayers, as reported previously [26, 43–45]. In this context, performing other experimental technique, such as nanoindentation and nanoscratch tests, would be beneficial to provide better understanding of the failure mechanisms of these layers [46–49]. The improvement of adhesion strength of multilayer coatings is attributed to the low morphological defects of the outer HA layer, as well as the possible enhancement of mechanical interlocking by the HA film and the substrate surface due to the increased roughness of TiO_2 structures. In addition, elemental intermixing and diffusion of calcium and phosphorous from the HA layer and titanium ions from the substrate into the TiO_2 interlayer during heat treatment, as demonstrated previously [20, 50], suggest the formation of chemical bonds at the TiO_2/substrate and HA/TiO_2 interfaces that could promote the adhesion of the bilayer. In summary, the results signify that the presence of TiO_2 interlayer improves the attachment HA coatings to the substrate surface making them more reliable in the load-bearing applications.

Corrosion of the Ti6Al4V implants leads to the release of metal ions into the body, specifically Al^{3+} and V^{5+}, that could cause allergic reactions when they interact with the surrounding tissues [9]. In addition, corrosion could deteriorate the mechanical properties of the implant surface [2]. Enhancing the anticorrosion property of Ti6Al4V implant is a requirement to be successfully applied in biomedical field, hence, the current work has investigated the influence of pure and substituted HA coatings on the corrosion resistance of titanium alloy in simulated body fluid. Figure 7 illustrates the polarization curves of the uncoated and coated substrates.

The electrochemical parameters for the uncoated and coated Ti6Al4V alloy are presented in Table 3. The corrosion potential values correlates with the thermodynamic aspect of the test, which describes the tendency of the coated substrate to corrode, while the value of the corrosion current density correlates with the kinetic aspect which indicates the corrosion rate of the coated specimen.

Generally, low I_{corr} and nobler E_{corr} values indicate low corrosion rate and better corrosion protection efficiency [51]. As expected, the uncoated alloy showed high I_{corr} value and low E_{corr} value proving its low corrosion resistance towards the solution in comparison to the coated samples. Application of HA coating reduced the I_{corr} and shifted E_{corr} to nobler values, which implies better chemical stability of the coated substrate against SBF solution. It has been indicated that the surface modification of the Ti6Al4V alloy improves its corrosion behavior due to the

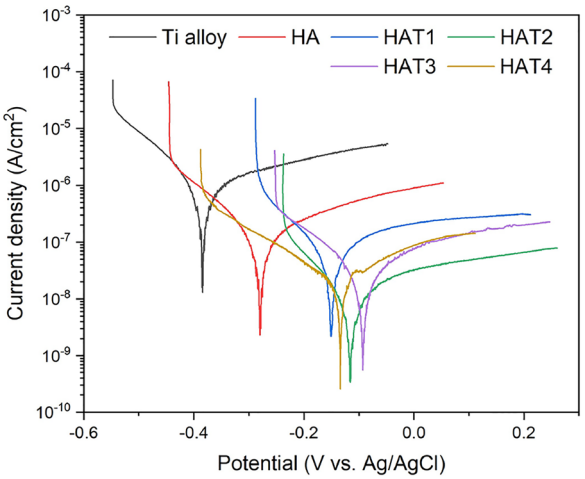

Figure 7: Potentiodynamic polarization curves of uncoated Ti6Al4V and various coatings in SBF solution.

TABLE 3: Corrosion potential, corrosion current and corrosion rate of uncoated Ti6Al4V and the indicated TiO_2 and HA coatings extracted from polarization curves.

Properties	Ti6Al4V	HA	HAT1	HAT2	HAT3	HAT4
E_{corr} (V)	− 0.384	− 0.271	− 0.151	− 0.116	− 0.093	− 0.133
I_{corr} (A cm^{-2})	9.04×10^{-7}	1.18×10^{-7}	5.91×10^{-8}	9.97×10^{-9}	2.56×10^{-8}	1.82×10^{-8}
CR (mm/y)	2.07×10^{-2}	2.70×10^{-3}	1.35×10^{-3}	2.28×10^{-4}	5.84×10^{-4}	4.15×10^{-4}

reduction of electron exchange between substrate and environment [52]. Introduction of different structures of TiO_2 interlayer further improved the corrosion resistance of the coated samples to a significant extent. In addition, the corrosion potentials of the bilayer coatings were remarkably shifted toward nobler values. These observations indicate the high protective property of HA/TiO_2 bilayer coatings due to the presence of TiO_2 interlayers, which act as a second barrier to prevent ion penetration from SBF into the underlying substrate. In addition, the high corrosion rate of the HA sample, compared to the HA/TiO_2 samples, could be related to the micro-cracks in the corresponding coatings as indicated in the previous section. These surface defects act as preferential sites for chloride ion penetration to reach the substrate surface. The reduced surface defects of the HA/TiO_2 coatings prevented the corrosive solution from penetrating the coating layer and reaching the substrate surface. The thickness of TiO_2 interlayer is an important factor which decrease the electric field and consequently reduce the electrical flux that finally results in lower I_{corr} values. Hence, the HAT2 and HAT4 samples with higher interlayer thickness compared to the other TiO_2 interlayer showed better corrosion resistance. In spite of the high interlayer thickness of the HAT1 coated samples, the cracks in the outer layer of these specimens could result in less corrosion resistance compared to other pretreated alloys. The current density reduction of the bilayer coating is partially attributed to the low electrical conductivity of the TiO_2 layer, which is hindering the transfer of charge carriers through the sample/electrolyte interface. In conclusion, the bilayer coatings significantly improve corrosion resistance and offer promising electrochemical properties for implant applications.

Conclusion

The present study has attempted to optimize the preparation process of hydroxyapatite coating and investigated the impact of the TiO_2 intermediate layers with different morphologies on the HA coating using different analytical methods. XRD analysis showed that aging the HA sol up to 72 h and adjusting its pH value to 7.6 play a vital role in production of single-phase HA, as well as elimination of non-biocompatible contaminants. In addition, the DSC/TG analysis indicated that 600 ℃ is an optimum sintering temperature to decompose organics and nitrates substances and produce crystalline HA. HA coating applied directly on the Ti6Al4V substrate has shown a cracked structure. However, introduction of TiO_2 interlayers has eliminated the morphological defects and improved the adhesive strength up to 76.2%. Results of the potentiodynamic polarization tests exhibit that the corrosion resistance is significantly improved for samples containing TiO_2 and that it is mainly affected by the thickness of the TiO_2 interlayer. It was clearly shown in this work that the inclusion of a TiO_2 interlayer to HA coated Ti6Al4V implants is very promising, since the improved adhesion of the HA layers to the substrate benefits from the modified morphology and an improved corrosion resistance. However, challenges still remain in the application of HA based multilayer in orthopedics due to its possible degradation in long-term implantations. Advances in research investigating long-term protection and stability of HA bilayers would give a better indication of the success of these coatings in orthopedic applications.

Methodology

Preparation of Ti6Al4V substrate

The Ti6Al4V rod (obtained from Horst Zu Jeddeloh, Germany) was cut into disk-shaped substrates (15 mm diameter, 5 mm thickness), then ground with SiC paper (1200 grit) to remove contaminations and macro defects, until a shiny appearance was achieved. Subsequently the samples were ultrasonically cleaned with acetone, ethanol and deionized water for 15 min each, and finally dried and stored in a desiccator for further use.

Formation of TiO_2 interlayer

TiO_2 by thermal oxidation (T1)

The TiO_2 interlayer produced by thermal oxidation was achieved by heating the Ti6Al4V samples at 450 °C with heating rate of 10 °C/min and held for 3 h. The samples were left to cool to room temperature.

TiO_2 by sol–gel coating (T2)

To achieve the TiO_2 sol, tetrabutylorthotitanate (Ti$(OCH_2CH_2CH_2CH_3)_4$; 98%, Merck) and diethanolamine ($HN(CH_2CH_2OH)_2$; 99.5%, Merck) were dissolved in ethanol. Due to the high reactivity of tetrabutylorthotitanate, introduction of ethanol could induce immediate precipitations.

Therefore, diethanolamine is initially mixed with ethanol to stabilize the hydrolysis process, then followed by tetrabutylorthotitanate addition. After 2 h of vigorous stirring, a mixture of ethanol and water was added dropwise, the resultant solution stirred for 2 h and aged for 24 h. The molar ratio of the used components were: $Ti(OC_4H_9)_4$:C_2H_5OH: $NH(C_2H_4OH)_2$:H_2O = 1:26.5:1:1 [53]. Dip coating of the samples was conducted in the TiO_2 sol at a withdrawal rate of 8 cm/min followed by heat treatment at 450 °C for 1 h in air. Part of this sol was used for preparation of powdered TiO_2 by initially drying at 80 °C for 12 h and sintering at 600 °C for 1 h.

TiO_2 by anodization (T3, T4)

The anodization process of the cleaned Ti6Al4V samples was done to produce TiO_2 layer as outlined in literature [27, 54, 55]. Briefly, the samples work as anodes while graphite rods were used as cathodes. Both electrodes were suspended in different electrolyte solutions applying two individual anodization processes. Firstly, sulfuric acid (H_2SO_4, 95%, Merck) as the electrolyte was used and a 50 V potential was applied for 5 min to produce TiO_2 layers with rough structure. Secondly, an electrolyte consisting of 90% ethylene glycol ($HOCH_2CH_2OH$; 99.8%, VWR), 9% DI water, 1% hydrofluoric acid (HF, 40%, Merck), and 0.25 wt% ammonium fluoride (NH_4F; 98% pure, Merck) was used with a potential of 60 V for 60 min to produce TiO_2 layers with micro-/nano-roughness structure. At the end of the processes, all anodized specimens were rinsed gently with DI water to remove excess electrolyte, then dried and stored in a desiccator for further investigations. The samples treated with fluoride-free and fluoride-containing electrolyte were coded as T3 and T4, respectively.

Preparation and deposition of HA sol

Triethyl phosphite ($(C_2H_5O)_3P$, 98% pure, Alfa Aesar) was initially mixed with ethanol and followed by addition of DI water for hydrolysis under vigorous stirring for 24 h in a sealed glass container. In this solution the molar ratios were H_2O:$(C_2H_5O)_3P$ = 4:1. 2 M of calcium nitrate tetrahydrate ($Ca(NO_3)_2$.4H2O; 99% pure, Merck) diluted in ethanol for 24 h was added dropwise into the hydrolyzed phosphite sol in stoichiometric amounts to achieve a ratio of Ca/P = 1.67. The transparency of the sol was retained during the drop mixing process, indicating a homogeneous solution containing a dissolved complex without any precipitate. After the mixing process, 2.5 and 5 vol% of ammonium hydroxide (NH_4OH; 32%, Merck) was added dropwise to the mixed solution which resulted in a pH increase up to 5.9 and 7.6, respectively. The mixed sol was continuously agitated for additional 2 h and then aged for 24, 48 and 72 h in static mode at room temperature. Part of these sols were used for preparation of powdered HA by initially drying at 80 °C for 12 h. The resulting gel was grounded by mortar and pestle into fine powder and subjected to a heat treatment at 600 °C (heating ramp: 5 °C/min, dwell time: 60 min, cool down rate: 10 °C/min). The prepared HA sol was deposited on the uncoated and TiO_2 precoated Ti6Al4V via dip coating at withdrawal speed of 8 cm/min. Afterwards, the samples were dried at 80 °C for 12 h and heat treated at 600 °C for 1 h resulting in the samples HA (without TiO_2) and HAT1-HAT4 (with respective to the TiO_2 interlayer).

Characterization

X-ray diffraction analysis (XRD, SEIFERT-FPM URD6 diffractometer) was performed on the HA powder to investigate the crystalline structure and phase composition. The device operated in symmetrical (θ–2θ) Bragg–Brentano mode and was equipped with a sealed X-ray tube with Cu anode (producing characteristic X-radiation with the wavelengths λ(Cu-Kα_1) = 1.54059 Å and λ(Cu-Kα_2) = 1.54443 Å). The diffracted beam passed a standard graphite monochromator removing unwanted radiation components before being registered by (0D) proportional counter. The sample was analyzed as a thin layer on a zero background holder [(510) cut Si single crystal]. Phase quantification was performed by Rietveld refinement method of XRD data collected over 2θ range 20°–80°.

Fourier transform infrared spectrometer (FTIR, Bruker Tensor II) was utilized to identify the functional groups of the HA powders using KBr pellet technique. The spectrum was collected in wavenumber range of 400–4000 cm^{-1} with a scanning resolution of 2 cm^{-1} and 16 scans at room temperature.

Thermal behavior of the HA dried gel was studied using differential scanning calorimetry analysis and thermogravimetric analysis (DSC/TG, NETZSCH). These investigations were performed in a temperature range from 25 to 800 °C with a scanning rate of 10 °C/min in alumina crucibles under atmospheric conditions.

Contact angle measurement using Kruss DSA25E goniometer was performed to estimate the wettability of the pretreated samples to DI water. Wetting of HA layers by SBF with a pH of 7.4 and at 37 ℃ with a drop volume of 2 µL was done. A lower contact angle could indicate the higher adhesion properties of the surface. The results are presented as mean ± standard deviation from ten measurements.

The surface morphology of the TiO_2 precoated Ti6Al4V samples and HA coated samples (with and without TiO_2) were investigated by scanning electron microscope (SEM, Phenom G2, Thermo Scientific). The thickness of TiO_2 and HA/TiO_2 layers was measured using non-contact film thickness measurement system (TF–C–UVIS–SR, StellarNet, USA) with 220–110 nm of wavelength

and resolution lower than 2.5 nm. The thickness measurements were carried out in range of 5 nm-20 µm and the results were presented as mean ± standard deviation from five measurements. While the average surface roughness of the TiO_2 and HA/TiO_2 bilayer samples were measured by surface profiler using a KLA-TENCOR.

The adhesive strength of the HA and HA/TiO_2 bilayer coatings on the Ti6Al4V surface was evaluated based on ASTM-C633 recommendations [56]. Briefly, the coated samples have been glued with epoxy resin to the surfaces of two titanium rods followed by curing at 150 ℃ for 1 h. A standard tensile test using a universal testing machine of model (WDW-200KN) at constant load speed rate of 1 mm/s was carried out. The bonding strength was determined as the maximum stress required to peel-off the coating layers, the data are presented as mean ± standard deviation ($n = 5$). Statistical analysis was performed between different groups by one-way analysis of variance (ANOVA) followed by post hoc Tukey's multiple comparison tests. P-values < 0.05 were considered as statistically significant.

In vitro experiment to assess the apatite formation ability of the HA coating was performed by immersing the HA coated Ti6Al4V sample in SBF at 37 ℃. The SBF has been prepared according to instructions of Kukubo and Takadama [57] to obtain a solution with ion concentrations nearly equal to those of human blood plasma. After immersion, the SBF was refreshed every 72 h. After 21 days of incubation, the samples were taken out of SBF, rinsed gently with DI water, and then dried in oven at 50 °C for 24 h. SEM was used to observe the morphology of the precipitates.

Potentiodynamic polarization measurements were carried out using a potentiostat (VSP, Bio-Logic Science Instruments) for evaluation of corrosion behavior. Each measurement was performed in SBF at 37 ℃ using the conventional three electrode configuration, with the sample as the working electrode, a platinum mesh as the counter and a saturated Ag/AgCl as the reference. The open circuit potential (OCP) was measured for 30 min and subsequently the potentiodynamic polarization was conducted in a potential range of ± 250 mV vs. E_{Corr} at scan rate of 0.1 mV/sec. The corrosion parameters were determined from the received polarization curves based on the Tafel extrapolation method. The corrosion rate (CR) of the tested samples obtained from the corrosion current density (I_{corr}) was calculated based on Eq. 2 [58]:

$$\mathrm{CR}\left[\mathrm{mm/year}\right] = 22.8\left[\left(\mathrm{mm} * \mathrm{cm}^2\right)/\left(y * 10^{-3}A\right)\right] \times I_{\mathrm{corr}}\left[10^{-3}\ \mathrm{A/cm}^2\right] \quad (2)$$

Acknowledgments

The authors gratefully acknowledge the technical support of Jörg Adam, Angela Reichel and Susann Rabe. Also, we would like to express our gratitude to Dr. Charlotte Ashworth-Güth for English proofreading.

Funding

Open Access funding enabled and organized by Projekt DEAL. This research was funded by European Social Fund, grant number 100380877. Parts of this work were financed through public funds from the Federal Ministry of Education and Research and the State of Saxony (SN0390002).

Data availability

The data presented in this study are available in article and supplementary information.

Declarations

Conflict of interest The authors declare no conflict of interest.

Open Access

Supplementary Information

The online version contains supplementary material available at https://doi.org/10.1557/s43578-022-00550-0.

References

1. B. Hou, Y. Liu, H. Chen, Y. Yang, In vitro bioactivity, bio-corrosion resistance and antibacterial property of laser cladded HA coatings with different content of ZnO on Ti-6Al-4V substrate. Mater. Res. (2019). https://doi.org/10.1590/1980-5373-MR-2018-0744
2. D. Gopi, E. Shinyjoy, M. Sekar, M. Surendiran, L. Kavitha, T.S. Sampath Kumar, Development of carbon nanotubes reinforced hydroxyapatite composite coatings on titanium by electrodeposition method. Corros. Sci. **73**, 321–330 (2013). https://doi.org/10.1016/j.corsci.2013.04.021
3. H. Jafari, H. Hessam, S.M.G. Shahri, M. Assadian, S.H.P. Shairazi-fard, M.H. Idris, Characterizing sintered nano-hydroxyapatite sol-gel coating deposited on a biomedical Ti-Zr-Nb alloy. J. Mater.

Eng. Perform. **25**(3), 901–909 (2016). https://doi.org/10.1007/s11665-016-1944-4

4. K. Pałka, R. Pokrowiecki, Porous titanium implants: a review. Adv. Eng. Mater. **20**(5), 1–18 (2018). https://doi.org/10.1002/adem.201700648
5. L.M. Wolford, Factors to consider in joint prosthesis systems. Baylor Univ. Med. Cent. Proc. **19**(3), 232–238 (2006). https://doi.org/10.1080/08998280.2006.11928170
6. A. Chandra et al., Life expectancy of modular Ti6Al4V hip implants: influence of stress and environment. J. Mech. Behav. Biomed. Mater. **4**(8), 1990–2001 (2011). https://doi.org/10.1016/j.jmbbm.2011.06.018
7. S. Noumbissi, A. Scarano, S. Gupta, A literature review study on atomic ions dissolution of titanium and its alloys in implant dentistry. Materials (Basel) **12**(3), 1–15 (2019). https://doi.org/10.3390/ma12030368
8. R.B. Heimann, H.D. Lehmann, *Bioceramic Coatings for Medical Implants: Trends and Techniques* (Wiley, New York, 2015)
9. A. Jaafar, C. Hecker, P. Árki, Y. Joseph, Sol-gel derived hydroxyapatite coatings for titanium implants: a review. Bioengineering **7**(4), 127 (2020). https://doi.org/10.3390/bioengineering7040127
10. B. Ben-Nissan, A. Milev, R. Vago, Morphology of sol-gel derived nano-coated coralline hydroxyapatite. Biomaterials **25**(20), 4971–4975 (2004). https://doi.org/10.1016/j.biomaterials.2004.02.006
11. Y.M. Lim, K.S. Hwang, Y.J. Park, Sol-gel derived functionally graded TiO2/HAP films on Ti-6Al-4V implants. J. Sol-Gel Sci. Technol. **21**(1–2), 123–128 (2001). https://doi.org/10.1023/A:1011230221011
12. K. Ishikawa, E. Garskaite, A. Kareiva, Sol–gel synthesis of calcium phosphate-based biomaterials—a review of environmentally benign, simple, and effective synthesis routes. J. Sol-Gel Sci. Technol. (2020). https://doi.org/10.1007/s10971-020-05245-8
13. S. Kannan, J.M.G. Ventura, A.F. Lemos, A. Barba, J.M.F. Ferreira, Effect of sodium addition on the preparation of hydroxyapatites and biphasic ceramics. Ceram. Int. **34**(1), 7–13 (2008). https://doi.org/10.1016/j.ceramint.2006.07.007
14. M. Sadat-Shojai, M.T. Khorasani, A. Jamshidi, Hydrothermal processing of hydroxyapatite nanoparticles—a Taguchi experimental design approach. J. Cryst. Growth **361**(1), 73–84 (2012). https://doi.org/10.1016/j.jcrysgro.2012.09.010
15. C.S. Chai, K.A. Gross, B. Ben-Nissan, Critical ageing of hydroxyapatite sol-gel solutions. Biomaterials **19**(24), 2291–2296 (1998). https://doi.org/10.1016/S0142-9612(98)90138-7
16. H.W. Kim, H.E. Kim, H.W. Kim, J.C. Knowles, Improvement of hydroxyapatite sol-gel coating on titanium with ammonium hydroxide addition. J. Am. Ceram. Soc. **88**(1), 154–159 (2005). https://doi.org/10.1111/j.1551-2916.2004.00030.x
17. K. Kang, H. Lim, K.D. Yun, S. Park, C. Jeong, K. Lee, Effect of viscosities on the surface morphology and crystallographic properties of hydroxyapatite coated titanium dioxide nanotubes. J. Nanosci. Nanotechnol. **15**(7), 5310–5313 (2015). https://doi.org/10.1166/jnn.2015.10395
18. H. Wang, C.Z. Chen, D.G. Wang, Effect of heating rate on structure of HA coating prepared by sol-gel. Surf. Eng. **25**(2), 131–135 (2009). https://doi.org/10.1179/026708409X364975
19. K.A. Gross, C.S. Chai, G.S. Kannangara, B. Ben-Nissan, L. Hanley, Thin hydroxyapatite coatings via sol–gel synthesis. J. Mater. Sci.: Mater. Med. **9**(12), 839–43 (1998)
20. H.W. Kim, Y.H. Koh, L.H. Li, S. Lee, H.E. Kim, Hydroxyapatite coating on titanium substrate with titania buffer layer processed by sol-gel method. Biomaterials **25**(13), 2533–2538 (2004). https://doi.org/10.1016/j.biomaterials.2003.09.041
21. A. Balakrishnan, B.C. Lee, T.N. Kim, B.B. Panigrahi, Strength and reliability performance of hydroxyapatite coatings on titania treated Ti6Al4V alloy using sol-gel precursor. Solid State Phenom. **124–126**(PART 2), 1161–1164 (2007). https://doi.org/10.4028/www.scientific.net/ssp.124-126.1161
22. R. Azari, H.R. Rezaie, A. Khavandi, Investigation of functionally graded HA-TiO2 coating on Ti–6Al–4V substrate fabricated by sol-gel method. Ceram. Int. **45**(14), 17545–17555 (2019). https://doi.org/10.1016/j.ceramint.2019.05.317
23. W. Xu, W. Hu, M. Li, C. Wen, Sol-gel derived hydroxyapatite/titania biocoatings on titanium substrate. Mater. Lett. **60**(13–14), 1575–1578 (2006). https://doi.org/10.1016/j.matlet.2005.11.072
24. S.M. Hussein, M.T. Mohammed, Pure and bilayer sol-gel nanolayers derived on a novel Ti surface for load bearing applications. Mater. Today Proc. **18**, 2217–2224 (2019). https://doi.org/10.1016/j.matpr.2019.07.001
25. R. Roest, B.A. Latella, G. Heness, B. Ben-Nissan, Adhesion of sol-gel derived hydroxyapatite nanocoatings on anodised pure titanium and titanium (Ti6Al4V) alloy substrates. Surf. Coat. Technol. **205**(11), 3520–3529 (2011). https://doi.org/10.1016/j.surfcoat.2010.12.030
26. X. Ji et al., Sol-gel-derived hydroxyapatite-carbon nanotube/titania coatings on titanium supstrates. Int. J. Mol. Sci. **13**(4), 5242–5253 (2012). https://doi.org/10.3390/ijms13045242
27. S.F. Robertson, A. Bandyopadhyay, S. Bose, Titania nanotube interface to increase adhesion strength of hydroxyapatite sol-gel coatings on Ti-6Al-4V for orthopedic applications. Surf. Coat. Technol. **372**, 140–147 (2019). https://doi.org/10.1016/j.surfcoat.2019.04.071
28. K. Kang, A. Zakiyuddin, K. Lee, Electrochemical properties of HA coated titanium dioxide nanotubes. J. Nanosci. Nanotechnol. **16**(2), 1708–1710 (2016). https://doi.org/10.1166/jnn.2016.11988
29. B.I. Baddar, A. Shah, H. Mas Ayu, R. Daud, M.S. Dambatta, Hydroxyapatite and thermal oxidation as intermediate layer on metallic biomaterial for medical implant: a review. J. Adv. Res. Fluid Mech. Therm. Sci. **62**(1), 138–150 (2019)

30. A. Balamurugan et al., Synthesis and structural analysis of SOL gel derived stoichiometric monophasic hydroxyapatite. Ceram. Silikaty **50**(1), 27–31 (2006)
31. D.M. Liu, T. Troczynski, W.J. Tseng, Water-based sol-gel synthesis of hydroxyapatite: process development. Biomaterials **22**(13), 1721–1730 (2001). https://doi.org/10.1016/S0142-9612(00)00332-X
32. H. Eshtiagh-Hosseini, M.R. Housaindokht, M. Chahkandi, Effects of parameters of sol-gel process on the phase evolution of sol-gel-derived hydroxyapatite. Mater. Chem. Phys. **106**(2–3), 310–316 (2007). https://doi.org/10.1016/j.matchemphys.2007.06.002
33. D. Wang, C. Chen, T. He, T. Lei, Hydroxyapatite coating on Ti6Al4V alloy by a sol-gel method. J. Mater. Sci. Mater. Med. **19**(6), 2281–2286 (2008). https://doi.org/10.1007/s10856-007-3338-5
34. M.H. Fathi, A. Hanifi, Sol-gel derived nanostructure hydroxyapatite powder and coating: aging time optimisation. Adv. Appl. Ceram. **108**(6), 363–368 (2009). https://doi.org/10.1179/174367609X414080
35. X.Z. Xue, J.Y. Zhang, D. Zhou, J.K. Liu, In-situ bonding technology and excellent anticorrosion activity of graphene oxide / hydroxyapatite nanocomposite pigment. Dye. Pigment **160**(2018), 109–118 (2019). https://doi.org/10.1016/j.dyepig.2018.07.057
36. K.Y. Hung, S.C. Lo, C.S. Shih, Y.C. Yang, H.P. Feng, Y.C. Lin, Titanium surface modified by hydroxyapatite coating for dental implants. Surf. Coat. Technol. **231**, 337–345 (2013). https://doi.org/10.1016/j.surfcoat.2012.03.037
37. A.A. El Hadad, E. Peón, F.R. García-Galván, V. Barranco, J. Parra, A. Jiménez-Morales, J.C. Galván, Biocompatibility and corrosion protection behaviour of hydroxyapatite sol-gel-derived coatings on Ti6Al4V alloy. Materials **10**(2), 94 (2017)
38. A. Jankovic et al., Bioactive hydroxyapatite/graphene composite coating and its corrosion stability in simulated body fluid Bioactive hydroxyapatite/graphene composite coating and its corrosion stability in simulated body fluid. J. Alloys Compd. **624**, 148–157 (2015). https://doi.org/10.1016/j.jallcom.2014.11.078 (**Contents**)
39. D. Gopi et al., Enhanced corrosion resistance of strontium hydroxyapatite coating on electron beam treated surgical grade stainless steel. Appl. Surf. Sci. **286**, 83–90 (2013). https://doi.org/10.1016/j.apsusc.2013.09.023
40. C.E. Wen, W. Xu, W.Y. Hu, P.D. Hodgson, Hydroxyapatite/titania sol-gel coatings on titanium-zirconium alloy for biomedical applications. Acta Biomater. **3**(3) SPEC. ISS, 403–410 (2007). https://doi.org/10.1016/j.actbio.2006.10.004.
41. S. Durdu, K. Korkmaz, S.L. Aktuğ, A. Çakır, Characterization and bioactivity of hydroxyapatite-based coatings formed on steel by electro-spark deposition and micro-arc oxidation. Surf. Coat. Technol. **326**, 111–120 (2017)
42. K. Prem Ananth, A. Joseph Nathanael, S.P. Jose, T.H. Oh, D. Mangalaraj, A novel silica nanotube reinforced ionic incorporated hydroxyapatite composite coating on polypyrrole coated 316L SS for implant application. Mater. Sci. Eng. C **59**, 1110–1124 (2016). https://doi.org/10.1016/j.msec.2015.10.045
43. M.S. Safavi, M. Etminanfar, A review on the prevalent fabrication methods, microstructural, mechanical properties, and corrosion resistance of nanostructured hydroxyapatite containing bilayer and multilayer coatings used in biomedical applications. J. Ultrafine Grained Nanostruct. Mater. **52**(1), 1–17 (2019). https://doi.org/10.22059/JUFGNSM.2019.01.01
44. Y. Yajing, D. Qiongqiong, H. Yong, S. Han, X. Pang, Magnesium substituted hydroxyapatite coating on titanium with nanotublar TiO_2 intermediate layer via electrochemical deposition. Appl. Surf. Sci. **305**, 77–85 (2014). https://doi.org/10.1016/j.apsusc.2014.02.163
45. R. Palanivelu, A.R. Kumar, Scratch and wear behaviour of plasma sprayed nano ceramics bilayer Al_2O_3–13 wt%TiO_2/hydroxyapatite coated on medical grade titanium substrates in SBF environment. Appl. Surf. Sci. **315**(1), 372–379 (2014). https://doi.org/10.1016/j.apsusc.2014.07.167
46. J. Chen, S.J. Bull, Approaches to investigate delamination and interfacial toughness in coated systems: an overview. J. Phys. D **44**(3), 034001 (2011). https://doi.org/10.1088/0022-3727/44/3/034001
47. G.P. Dinda, J. Shin, J. Mazumder, Pulsed laser deposition of hydroxyapatite thin films on Ti-6Al-4V: effect of heat treatment on structure and properties. Acta Biomater. **5**(5), 1821–1830 (2009). https://doi.org/10.1016/j.actbio.2009.01.027
48. S. Saber-Samandari, K.A. Gross, Nanoindentation reveals mechanical properties within thermally sprayed hydroxyapatite coatings. Surf. Coatings Technol. **203**(12), 1660–1664 (2009). https://doi.org/10.1016/j.surfcoat.2008.12.025
49. A. Karimzadeh, M.R. Ayatollahi, A.R. Bushroa, M.K. Herliansyah, Effect of sintering temperature on mechanical and tribological properties of hydroxyapatite measured by nanoindentation and nanoscratch experiments. Ceram. Int. **40**(7) PART A, 9159–9164 (2014). https://doi.org/10.1016/j.ceramint.2014.01.131
50. C.J. Tredwin, G. Georgiou, H.W. Kim, J.C. Knowles, Hydroxyapatite, fluor-hydroxyapatite and fluorapatite produced via the sol-gel method: Bonding to titanium and scanning electron microscopy. Dent. Mater. **29**(5), 521–529 (2013). https://doi.org/10.1016/j.dental.2013.02.002
51. O. Yigit, N. Ozdemir, B. Dikici, M. Kaseem, Surface properties of graphene functionalized TiO_2/nHA hybrid coatings made on Ti6Al7Nb alloys via plasma electrolytic oxidation (PEO). Molecules **26**(13), 3903 (2021)
52. S.A.X. Stango, D. Karthick, S. Swaroop, U.K. Mudali, U. Vijayalakshmi, Development of hydroxyapatite coatings on laser textured 316 LSS and Ti-6Al-4V and its electrochemical behavior

in SBF solution for orthopedic applications. Ceram. Int. **44**(3), 3149–3160 (2018). https://doi.org/10.1016/j.ceramint.2017.11.083

53. R.C. Suciu, M.C. Roşu, T.D. Silipaş, A.R. Biriş, I. Bratu, E. Indrea, TiO2 thin films prepared by spin coating technique. Rev. Roum. Chim. **56**(6), 607–612 (2011)
54. D. Velten, V. Biehl, F. Aubertin, B. Valeske, W. Possart, J. Breme, Preparation of TiO2 layers on cp-Ti and Ti6Al4V by thermal and anodic oxidation and by sol-gel coating techniques and their characterization. J. Biomed. Mater. Res. **59**(1), 18–28 (2002). https://doi.org/10.1002/jbm.1212
55. M.L. Vera, M.R. Rosenberger, C.E. Schvezov, A.E. Ares, Fabrication of TiO_2 crystalline coatings by combining Ti-6Al-4V anodic oxidation and heat treatments. Int. J. Biomater. (2015). https://doi.org/10.1155/2015/395657
56. S.T. Method, Standard test method for adhesion or cohesion strength of thermal spray coatings 1. Current **03**(2008), 1–7 (2001)
57. T. Kokubo, H. Takadama, How useful is SBF in predicting in vivo bone bioactivity? Biomaterials **27**(15), 2907–2915 (2006). https://doi.org/10.1016/j.biomaterials.2006.01.017
58. Y. Huang et al., Corrosion resistance and cytocompatibility studies of zinc-doped fluorohydroxyapatite nanocomposite coatings on titanium implant. Ceram. Int. **42**(1), 1903–15 (2016)